How to cite: *Angew. Chem. Int. Ed.* **2022,** *61,* e202210859
International Edition: doi.org/10.1002/anie.202210859
German Edition: doi.org/10.1002/ange.202210859

Li Metal Batteries

The Anionic Chemistry in Regulating the Reductive Stability of Electrolytes for Lithium Metal Batteries

Nan Yao[+], Shu-Yu Sun[+], Xiang Chen, Xue-Qiang Zhang, Xin Shen, Zhong-Heng Fu, Rui Zhang, and Qiang Zhang**

Abstract: Advanced electrolyte design is essential for building high-energy-density lithium (Li) batteries, and introducing anions into the Li^+ solvation sheaths has been widely demonstrated as a promising strategy. However, a fundamental understanding of the critical role of anions in such electrolytes is very lacking. Herein, the anionic chemistry in regulating the electrolyte structure and stability is probed by combining computational and experimental approaches. Based on a comprehensive analysis of the lowest unoccupied molecular orbitals, the solvents and anions in Li^+ solvation sheaths exhibit enhanced and decreased reductive stability compared with free counterparts, respectively, which agrees with both calculated and experimental results of reduction potentials. Accordingly, new strategies are proposed to build stable electrolytes based on the established anionic chemistry. This work unveils the mysterious anionic chemistry in regulating the structure–function relationship of electrolytes and contributes to a rational design of advanced electrolytes for practical Li metal batteries.

Introduction

Throughout the history of human energy utilization, the easy access to fossil fuels including coal, oil, and natural gas gradually made these energy sources overwhelm firewood and predominate in the world energy consumption structure. Along with this comes the energy crisis and environmental pollution such as carbon emissions. Consequently, great efforts have been devoted to reviving the exploration and utilization of renewable energy in pursuit of resolving both environmental issues and energy demands for a sustainable society.[1] Electricity generated from renewables further bridges the primary energy sources and end-users, during which energy storage devices shoulder the responsibility to reserve these intermittent and distributed energies.[2] Lithium (Li) ion batteries (LIBs), as the representative of energy storage devices, have prevailed for many years owing to their superiority in energy density and portability.[3] Nowadays, the extension of application scenarios from pocket electronics to electric vehicles raises attention to Li metal batteries (LMBs) with a promising energy density beyond routine LIBs.[4,5]

Despite the advantage of high theoretical energy density, LMBs are seriously plagued by the high reactivity of the Li metal anode.[6] Parasitic reactions between Li metal anodes and liquid electrolytes are much more severe than those in traditional graphite-based LIBs, which not only consume electrolytes and active Li but also may generate flammable gases.[7] The depletion of active components and potential safety risks eventually lead to battery failure. Constructing a stable and uniform solid electrolyte interphase (SEI) on anodes has been widely considered as a dominant and effective solution to the above issues since it can prevent continuous side reactions between electrolytes and Li metal anodes, and render uniform Li deposition.[5,8]

The composition, structure, and physicochemical property of SEI are highly dependent on the solvation structure of electrolytes,[9] as solvents and salt anions in the Li-ion (Li^+) solvation sheath preferentially decompose on the anode surface, and their decomposition products ultimately constitute SEI.[10,11] Strategies involving the regulation of Li^+ solvation sheath are thus put forward to construct stable and high-ionic-conductivity SEI, represented by introducing new electrolyte components[12,13] and tailoring their proportions.[13,14] Especially, an inorganic-rich SEI attributed to the reduction of anion-participated Li^+ solvation sheaths (contact ion pairs and aggregates) has been demonstrated to favor fast Li^+ diffusion in SEI, endowing LMBs with uniform Li deposition and long-term cyclability.[15]

The introduction of anions into Li^+ solvation sheaths outwardly increases the probability of anions encountering the Li metal anode and getting reduced. The decomposed inorganic products prove to assist in improving the uniformity of SEI and battery performance.[16] However, the

[*] N. Yao,[+] S.-Y. Sun,[+] Dr. X. Chen, Dr. X. Shen, Dr. Z.-H. Fu, Prof. Q. Zhang
Beijing Key Laboratory of Green Chemical Reaction Engineering and Technology, Department of Chemical Engineering, Tsinghua University
Beijing 100084 (China)
E-mail: xiangchen@mail.tsinghua.edu.cn
zhang-qiang@mails.tsinghua.edu.cn
Dr. X.-Q. Zhang, Dr. R. Zhang
Advanced Research Institute for Multidisciplinary Science, Beijing Institute of Technology
Beijing 100081 (China)
and
School of Materials Science and Engineering, Beijing Institute of Technology
Beijing 100081 (China)
[+] These authors contributed equally to this work.

underlying functionality and effect of anions in Li^+ solvation sheaths have not been thoroughly investigated including the chemical origin of the preferential decomposition of anions in Li^+ solvation sheaths and the advantageous molecular structures of anions that favor producing inorganic fragments.[17] Therefore, it is essential to probe the anionic chemistry, which is also an important part of the solvation chemistry, to inspire a universal design principle for anions and electrolyte recipes.

In this contribution, the anionic chemistry in regulating the reductive stability of electrolytes is probed by combining multi-scale simulations and experimental characterizations. According to the lowest unoccupied molecular orbital (LUMO) analyses, the anion and solvent exhibit decreased and improved reductive stability, respectively, as long as the anion participates in the solvation sheath of Li^+ (Figure 1). In addition, the anion preferentially accepts the electron compared with the solvent during the single-electron reduction reaction, which leads to the rise of the anionic reduction potential. The calculation results are further verified by the linear sweep voltammetry (LSV) test that anions in Li^+ solvation exhibit a higher reduction potential than free anions. A LiF-rich SEI is accordingly formed as a result of the favored decomposition of anions, delivering efficient Li stripping/plating. These results highlight the significant role of anionic chemistry in regulating electrolyte stability by both facilitating anion reduction and preventing solvent reduction, inspiring fancy and promising strategies of rational electrolyte design for building stable LMBs.

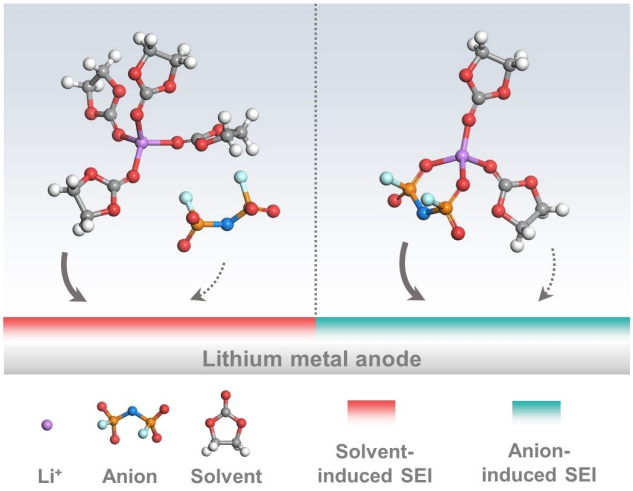

Figure 1. Schematic illustration of the anion participating in the Li^+ solvation sheath and corresponding influences. The entry of anions into Li^+ solvation sheaths results in the decreased reductive stability of anions and increased reductive stability of solvents, further inducing the formation of distinct solid electrolyte interphases. The bold solid and light dotted arrows represent the relatively higher and lower reductive stability of the same species, respectively.

Results and Discussion

Modeling and Frontier Molecular Orbital Theory Analyses. Electrolytes generally consist of organic solvents and Li salts. Herein typical solvents and salt anions used in LMBs are selected as the modeling system, including vinylene carbonate (VC), fluoroethylene carbonate (FEC), ethylene carbonate (EC), propylene carbonate (PC), acetonitrile (AN), 1,2-dimethoxyethane (DME), 1,3-dioxolane (DOL), dimethyl carbonate (DMC), ethyl methyl carbonate (EMC), and diethyl carbonate (DEC) solvents, and bis(fluorosulfonyl)imide (FSI^-), bis(trifluoromethanesulfonyl)imide ($TFSI^-$), nitrate (NO_3^-), and hexafluorophosphate (PF_6^-) ions. In low-concentration electrolytes, Li^+ is largely solvated by solvents. As the salt concentration increases, salt anions gradually participate in the solvation sheath of Li^+. Therefore, two electrolyte solvation structures, *i.e.*, Li^+–solvent (Figure S1) and Li^+–solvent–anion (Figures S2–5) complexes, are further considered. Through the comparison of the two models, the anionic chemistry in the electrolyte stability can be revealed.

The negative binding energy (E_b) between the Li^+–solvent complex and anion implies the thermodynamic stability when the anion takes part in the solvation sheath (Figure S6). For Li^+–solvent–anion complexes with different anions, the binding energies follow the order of $PF_6^- < FSI^- < TFSI^- < NO_3^-$, which is consistent with the binding energy trend between a Li^+ and an anion.[18] It is reasonable to observe such conformity since anions in Li^+–solvent–anion solvation sheaths primarily interact with the Li^+. Besides, solvents possessing low and high dielectric constant values have mild and significant solvation effects on the binding energy, respectively (Table S1).[19] That is why the binding energies of complexes with the same anion but different solvent types follow the order of cyclic carbonate $\approx$ AN < ether < linear carbonate.

To probe the anionic chemistry in manipulating the electrolyte stability, the LUMO energy level change (ΔLUMO) of both solvents and anions when introducing an anion into a Li^+ solvation sheath was further analyzed. On the one hand, the LUMO energy level of anions in Li^+–solvent–anion complexes reduces compared with that of free anions (Figure 2a). This can be attributed to the electron-withdrawing effect of positively charged Li^+, as evidenced by the increased charge of anions (Figure S7). For instance, the charge of NO_3^- becomes less negative by approximately 0.06 e^- when it coordinates with Li^+–DMC, signifying its loss of electrons. The LUMO energy level of NO_3^- accordingly reduces by around 1.49 eV. Besides, the change of anionic charge follows the order of $PF_6^- < FSI^- < TFSI^- < NO_3^-$, which is in line with the trend of the binding energy between the Li^+–solvent complex and anion. On the other hand, anions share the burden of such an electron-withdrawing effect with solvents, resulting in the increased LUMO energy level of solvents in Li^+–solvent–anion complexes than Li^+–solvent counterparts (Figure S8).

The ΔLUMO of anions and solvents is further correlated with the binding energy between a Li^+–solvent complex and an anion to understand the difference among various

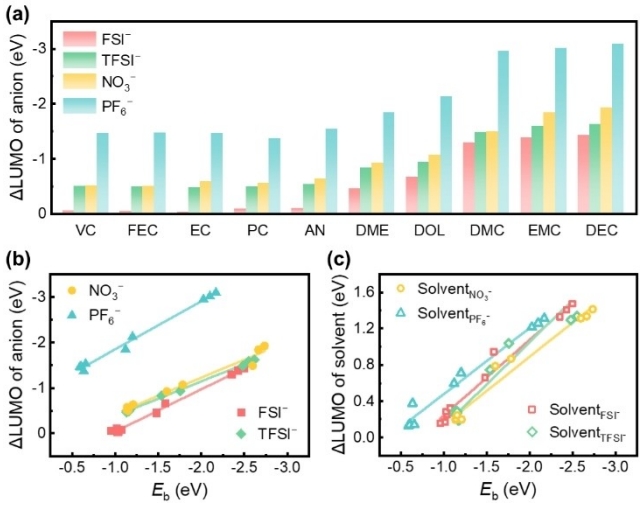

Figure 2. The energy level change of the lowest unoccupied molecular orbital (ΔLUMO) and its correlation with the binding energy (E_b). a) The ΔLUMO of anions before and after interacting with Li^+–solvent complexes. The correlation between the E_b and ΔLUMO of b) anions and c) solvents.

solvents and anions. A linear relationship between the ΔLUMO and binding energy is obtained for a specific anion (Figure 2b), which is similar to the results in Li^+–solvent complexes that the ΔLUMO of ether solvents delivers a linear relationship with the binding energy.[11] A larger binding energy corresponds to a stronger interaction between the Li^+ and anion, and therefore the Li^+ is easier to attract more electrons from the anion. The occupancy of electrons influences the LUMO energy level and its change, namely ΔLUMO. The more electrons Li^+ attracts, the larger decrease of the LUMO of anion is and the more negative ΔLUMO becomes. Meanwhile, the Li^+ attracts fewer electrons from the solvent because it becomes less positively charged after attracting electrons from the anion. The LUMO of the solvent becomes higher accordingly, and ΔLUMO of the solvent is also linearly correlated with the binding energy (Figure 2c). Furthermore, the linear relationship for different anions varies to some degree. For instance, PF_6^- has the smallest binding energy with Li^+–solvent among four anions but ΔLUMO of PF_6^- apparently exceeds the other three anions (Figure 2a and b). The LUMO of PF_6^- consists of P–F and PF_6^- interacts with Li^+ directly through the F atom (Figures S5 and 9), which gives rise to the large ΔLUMO of PF_6^- even though the binding energy is relatively small. Contrarily, the atoms that compose the LUMO of NO_3^-, FSI^-, and $TFSI^-$ do not interact with a Li^+ directly. Specifically, the N–O bond constitutes the LUMO of NO_3^- while the other two O atoms bind with Li^+, and the S–F and S–C bonds compose the LUMO of FSI^- and $TFSI^-$, respectively, while O atoms tend to interact with Li^+. Therefore, ΔLUMO of NO_3^-, FSI^-, and $TFSI^-$ is relatively insignificant though their corresponding binding energies and changes of charge are larger than those of PF_6^-. On the other hand, ΔLUMO of solvents has no definite order probably due to the combined effects of Li^+–solvent and Li^+–anion interactions. For instance, ΔLUMO of solvents in Li^+–solvent–NO_3^- is not the most significant despite the strongest binding energy of Li^+–solvent and NO_3^- among four anions (Figure S8). The delocalized π_4^6 bond in NO_3^- enables a highly dispersed electron distribution of NO_3^- and thus a strong electron-withdrawing ability, which induces electron feedbacks from Li^+ and solvent to NO_3^- and further delivers a strong interaction between NO_3^- and Li^+–solvent complexes. As a result, the electron-withdrawing effect of Li^+ on solvents is only slightly weakened, giving rise to less obvious ΔLUMO of solvents.

Reduction Potential Analyses. The decreased LUMO energy level of anions implies that the participation of anions in the Li^+ solvation sheath can cause the reduced reductive stability of anions themselves, while the increased LUMO energy level of solvents suggests the enhanced reductive stability of solvents. A single-electron reduction reaction was further considered to verify the change in the reductive stability. An extra electron was added to the Li^+–solvent–anion complexes. The distribution of this singly unpaired electron is deduced from the spin population analysis, which can reflect the electron affinity of species in the Li^+ solvation sheath. Taking Li^+–DMC–anion as an example, Figure 3a shows that atoms of FSI^-, $TFSI^-$, NO_3^-, and PF_6^- in the solvation sheath occupy over 90 % of the single electron, and anions are thus reduced with the bending of structure or even the breaking of chemical bonds (Figure 3b and Figure S10). The single electron is mainly accepted by the S atom for FSI^-. The bond length of S–F is then enlarged from about 1.65 Å to over 4.50 Å in most cases (Figure S10a), which suggests the breaking of the S–F bond. The decomposed F atom binds with Li^+ to form LiF, which is a very important component of SEI in working batteries.[13,20] Circumstances of PF_6^- are similar to those of FSI^-. The electron fills in the P atom, and the P–F bond is broken with the bond length increasing by around 3.00 Å to produce LiF (Figure S10b). Differently, N and O of FSI^- also accept a large proportion of electron and FSI^- will probably continue to decompose.[21] The PF_5 formed from PF_6^- losing one F atom is relatively stable because the added electron is almost occupied by the P atom.[22] S, C, and F atoms of $TFSI^-$ share the electron, and $TFSI^-$ also undergoes the S–C bond breaking (Figure S10c). For NO_3^-, N and O (O atoms that do not directly interact with Li^+) atoms accept the electron. The resonance structure due to the π bond renders NO_3^- only deform without degrading.

Consistent with the spin population analysis, the charge of atoms accepting the electron becomes more negative except that the atomic charge of F in FSI^- and PF_6^- visibly changes as well while that of C in $TFSI^-$ does not show distinct changes (Figure 3c). F atoms of FSI^- and PF_6^- initially bond with S or P atoms, but they turn to form LiF during the reduction process. The chemical bond transforms from a covalent bond to an ionic bond. F atoms can receive more electrons, and consequently, the atomic charges are significantly reduced. The C of $TFSI^-$ forms a covalent bond with S, where two electrons are shared by these two atoms. After the C occupies the single electron and is separated from S, it still possesses two electrons, which rationalizes its

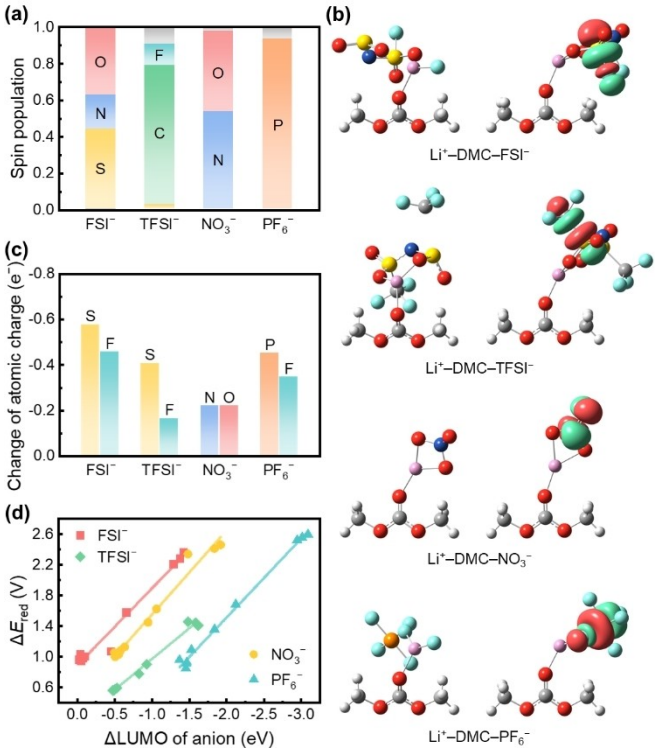

Figure 3. The spin population, structural change, atomic charge, and reductive potential analyses of the single-electron reduction reaction of Li^+–DMC–anion complexes. a) The spin population values of anions in reduced Li^+–DMC–anion complexes. b) The optimized geometrical structures of reduced Li^+–DMC–anion complexes and visualized LUMOs of anions in original complexes. White, pink, grey, blue, red, cyan, orange, and yellow balls represent H, Li, C, N, O, F, P, and S atoms, respectively. Red and green regions of LUMOs represent the positive and negative parts of orbitals, respectively (isovalue: 0.05 e^- $Bohr^{-3}$). c) The change of atomic charge when Li^+–DMC–anion complexes accept one electron. d) The correlation between ΔLUMO and reduction potential change of anions.

negligible charge change. The same change in spin population and atomic charge holds true for other solvent systems (Figure S11). Atomic sites where the electron filling, structural change, and change of charges take place are in correspondence with the LUMO composition (Figure 3a–c and Figures S11–19), demonstrating LUMO as an effective indicator of reductive stability.

Since anions are primary electron acceptors, the calculated reduction potential (E_{red}) of Li^+–solvent–anion can be viewed as the anionic reduction potential and compared with that of free anions. The difference between these two reduction potential values ($\Delta E_{red} = E_{red,Li^+\text{-solvent-anion}} - E_{red,free\ anion}$) is positive, which manifests the reduced reductive stability of anions after entering the Li^+ solvation sheath (Figure 3d). ΔE_{red} is also linearly related to ΔLUMO of anions. A larger change of LUMO corresponds to a larger ΔE_{red} for the same anion with the slope of the fitting curve very close to 1.00, which matches the single-electron reduction reaction. This also implies that LUMO is the place accommodating the added electron, and LUMO and ΔLUMO are qualified to evaluate the reductive stability and its alteration. For different anions, ΔE_{red} is not as large as ΔLUMO. For example, the difference of ΔLUMO between FSI^- and PF_6^- in Li^+–DMC is 1.66 eV but the difference of ΔE_{red} is only 0.31 V. This is probably due to the different LUMO compositions (i.e., S–F, S–C, N–O, and P–F for FSI^-, $TFSI^-$, NO_3^-, and PF_6^-, respectively) and the tendency of these sites to be reduced.

Experimental Verifications. Experimentally, the electrolyte stability is widely determined by the LSV test, which was further considered in this work to verify the theoretical results above. In order to demonstrate that anions in Li^+ solvation sheaths have a higher reduction potential and lower reductive stability than free anions, a series of model electrolytes are constructed by regulating the salt concentration. Many experimental and computational studies have confirmed that the association between Li^+ and anions is strengthened with increasing salt concentrations.[23] Free anions and solvated Li^+ completely coordinated by solvents are the majority in low-concentration electrolytes, while a large proportion of anion-participated solvation sheaths exist in high-concentration electrolytes. According to molecular dynamics (MD) simulations on 0.1, 1.0, and 2.0 M LiFSI/EC/DMC (EC:DMC = 1:1 in vol %) electrolytes, more FSI^- take part in Li^+ solvation sheaths with the coordination number of FSI^- increasing from 0.31 to 0.63 and 1.58 when the salt concentration increases from 0.1 to 1.0 and 2.0 M (Figure 4a–c and Figure S17). Nearly 80 % of solvation structures in 0.1 M LiFSI/EC/DMC have no anion involved but this value declines to 56 % and 22 % in 1.0 and 2.0 M electrolytes, respectively (Figure 4d). Simultaneously, solvation structures containing more than one anion occupy a growing proportion when the salt concentration increases. Therefore, electrolytes with three salt concentrations ranging from low to high, *i.e.*, 0.1, 1.0, and 2.0 M, are used to probe the anionic chemistry in regulating electrolyte reductive stability. The point on the LSV curve where the derivative of current density with respect to the potential starts deviating from zero is considered as the reduction potential of anions. Figure 4e depicts the reductive potentials of FSI^- in 0.1, 1.0, and 2.0 M LiFSI/EC/DMC are 1.29, 1.35, and 1.44 V, respectively, which agrees with results obtained from the above DFT calculations that anions are less reductively stable once they participate in the solvation of Li^+.

The depth profile of SEI obtained from X-ray photoelectron spectroscopy (XPS) further discloses that the decreased reductive stability (increased reductive potential) of anions favors the formation of inorganic-rich SEI (Figure 4f and Figure S18). Specifically, after sputtering, F accounts for less than 2 % of atomic distributions in SEI formed in the 0.1 M electrolyte. This value rises to around 7 % and 15 % when FSI^- becomes more reducible at high salt concentrations. The F components are mainly identified as LiF, verifying the calculated single-electron reduction reaction where F atoms tend to be decomposed from FSI^- and bind with Li^+ to form LiF (Figure 3b). A LiF-rich SEI is beneficial for stabilizing the electrolyte–electrode interface and minimizing parasitic reactions. Therefore, the Li||Cu battery with 2.0 M electrolyte delivers a higher Coulombic

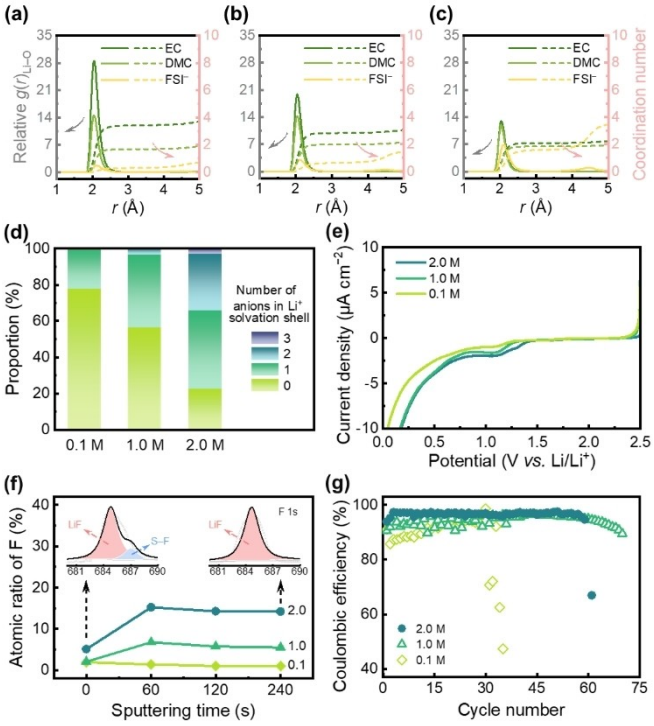

Figure 4. The solvation structures and electrochemical properties of LiFSI/EC/DMC electrolytes. The relative radial distribution function ($g(r)$) and coordination number of electrolytes with a) 0.1 M, b) 1.0 M, and c) 2.0 M LiFSI. d) The distribution of solvation structures containing different numbers of anions. e) LSV curves of electrolytes with different salt concentrations. f) The evolution of the atomic ratio of F with the sputtering time and XPS spectra of F 1s (inset figure, the bottom axis is the binding energy in the unit of eV). g) CE of Li||Cu batteries containing electrolytes with different salt concentrations. The volume ratio of EC and DMC is 1:1.

efficiency (CE) than those with 0.1 and 1.0 M electrolytes, especially during the first 20 cycles (Figure 4g). The battery containing 0.1 M LiFSI/EC/DMC failed at 30 cycles due to its least stable SEI. The 1.0 M electrolyte had a narrowly leading cycling performance compared with the 2.0 M electrolyte, which can be attributed to the fragile nature of the inorganic-rich SEI. Besides, these electrolytes are further applied to practical Li||$LiNi_{0.5}Co_{0.2}Mn_{0.3}O_2$ (NCM523) batteries. The battery with the 2.0 M electrolyte exhibits a longer cycling life than those with low-concentration electrolytes (Figure S22). The 0.1 and 1.0 M batteries fail at around 10 and 15 cycles, respectively, at 80 % capacity retention, while the 2.0 M battery merely shows minor degradation at 30 cycles, demonstrating the significance of anions in building a durable SEI for Li metal anodes.

Electrolyte Design Strategies. Regulating the chemical structure and solvation structure of anions has been widely demonstrated as one of the most effective and promising strategies for designing advanced electrolytes for LMBs in experiments. The anionic chemistry built in this work not only uncovers the underlying chemical mechanism of such a strategy deeply and comprehensively but also affords fruitful insights into the rational design of advanced electrolytes at the atomic level:

(1) **Conjugate Structure Design**. Anions with a conjugate functional group are supposed to deliver a strong interaction with a Li^+ and further weaken the interaction between solvents and the Li^+. As a result, the reductive stability of both solvents and anions can be improved. Such conjugate effect rationalizes the strongest interaction with a Li^+ but the best reductive stability of NO_3^- among four anions considered in this work. Therefore, constructing a similar conjugate functional group to NO_3^- is supposed to be a promising anionic design strategy.

(2) **LUMO Regulation**. The LUMO composition and energy level are important parameters for anion design. On the one hand, anions with a low LUMO energy level are supposed to decompose easily and deliver a large contribution to the SEI formation. On the other hand, atoms of anions that constitute the LUMO should interact with a Li^+ directly in the solvation structure to further promote such reduction decomposition. Promising SEI components like LiF thus can be delicately introduced by designing such counterparts in anions. Contrarily, stable anions with high-energy-level LUMO and corresponding LUMO atoms not involved in coordinating with a Li^+ can be designed.

(3) **Synergy between Anions and Solvents**. The synergistic effect between anions and solvents plays a decisive role in determining electrolyte stability, which can be fully understood through the ion–solvent chemistry. Cations and anions can decrease and increase the LUMO energy level of solvents, respectively. In practical electrolytes, the solvation structure of Li^+ often consists of both solvents and anions. Electrolyte design singly from the solvent or anion side is not sufficient, especially for the emerging high-throughput screening and machine-learning paradigms. It is highly recommended to consider the electrolyte design based on the overall solvation structures, *i.e.*, ion–solvent complexes. In this way, the (average) binding energy between ions and solvents and the LUMO evolution of each component in the complexes can serve as highly effective and practical parameters to be fed into a high-throughput and rational design of advanced electrolytes. It also should be noted that certain lithium salt has limited solubility in selected solvents, which restricts the interaction between Li^+ and solvents. Therefore, the salt solubility is supposed to be considered when regulating solvation structures or taking advantage of the synergy between anions and solvents.

Conclusion

The anionic chemistry in electrolytes for Li metal batteries is investigated by both theoretical calculations and experimental tests based on typical organic solvents and salt anions. Especially, the working mechanism of anions in regulating the reductive stability of anions and solvents in Li^+ solvation sheaths is unveiled at the molecular and electronic levels. The LUMO energy level of solvents

becomes higher and that of anions becomes lower when anions coordinate with a Li^+–solvent complex. This indicates the participation of anions in Li^+ solvation sheaths not only improves the reductive stability of solvents but also promotes the reduction of anions themselves. The single-electron reduction reaction further embodies the higher electron affinity of anions compared with solvents. Anions in Li^+ solvation sheaths are prone to accept the electron and get reduced, favoring the formation of inorganic species such as LiF. The corresponding reductive potential also increases as the reductive potential of free anions, which is consistent with the decreased anionic reductive stability demonstrated by both LUMO energy level results and LSV tests. Additionally, the change of the anionic reductive potential ΔE_{red} is in a linear relationship with ΔLUMO, which corroborates the effectiveness of LUMO in estimating the reductive stability. This work reveals the working mechanism and important role of anions in regulating the reductive stability of both anions and solvents in Li^+ solvation sheaths and deepens the understanding of the derivation of inorganic-rich SEI. The demonstrated anionic chemistry not only helps to deliver a rational design of advanced electrolytes for practical Li metal batteries but also applies to other energy storage devices such as sodium and potassium batteries.

Acknowledgements

This work was supported by the Beijing Municipal Natural Science Foundation (Z200011), National Key Research and Development Program (2021YFB2500300), National Natural Science Foundation of China (22109086, U1801257, and 21825501), China Postdoctoral Science Foundation (2021TQ0161 and 2021M691709), Young Elite Scientists Sponsorship Program by CAST (2021QNRC001), and Grant 2020GQG1006 from the Guoqiang Institute at Tsinghua University. The authors acknowledged the support from Tsinghua National Laboratory for Information Science and Technology for theoretical simulations. X. Chen appreciates the support from the Shuimu Tsinghua Scholar Program of Tsinghua University.

Conflict of Interest

The authors declare no conflict of interest.

Data Availability Statement

The data that support the findings of this study are available from the corresponding author upon reasonable request.

Keywords: anionic chemistry · solvation chemistry · electrolyte stability · lithium metal battery · multi-scale simulation

[1] International Energy Agency, France, **2020**.
[2] D. Larcher, J.-M. Tarascon, *Nat. Chem.* **2015**, *7*, 19–29.
[3] M. Li, J. Lu, Z. Chen, K. Amine, *Adv. Mater.* **2018**, *30*, 1800561; V. Giordani, D. Tozier, J. Uddin, H. Tan, B. M. Gallant, B. D. McCloskey, J. R. Greer, G. V. Chase, D. Addison, *Nat. Chem.* **2019**, *11*, 1133–1138.
[4] X.-B. Cheng, R. Zhang, C.-Z. Zhao, Q. Zhang, *Chem. Rev.* **2017**, *117*, 10403–10473; J.-l. Ma, F.-l. Meng, Y. Yu, D.-p. Liu, J.-m. Yan, Y. Zhang, X.-b. Zhang, Q. Jiang, *Nat. Chem.* **2019**, *11*, 64–70; J. F. Ding, R. Xu, C. Yan, B. Li, H. Yuan, J. Huang, *J. Energy Chem.* **2021**, *59*, 306–319; F. N. Jiang, S. J. Yang, H. Liu, X. B. Cheng, L. Liu, R. Xiang, Q. Zhang, S. Kaskel, J. Q. Huang, *SusMat* **2021**, *1*, 506–536; F. Li, J. He, J. D. Liu, M. G. Wu, Y. Y. Hou, H. P. Wang, S. H. Qi, Q. H. Liu, J. W. Hu, J. M. Ma, *Angew. Chem. Int. Ed.* **2021**, *60*, 6600–6608; *Angew. Chem.* **2021**, *133*, 6674–6682; S. Y. Yuan, T. Y. Kong, Y. Y. Zhang, P. Dong, Y. J. Zhang, X. L. Dong, Y. G. Wang, Y. Y. Xia, *Angew. Chem. Int. Ed.* **2021**, *60*, 25624–25638; *Angew. Chem.* **2021**, *133*, 25828–25842.
[5] J.-G. Zhang, W. Xu, J. Xiao, X. Cao, J. Liu, *Chem. Rev.* **2020**, *120*, 13312–13348.
[6] D. Lin, Y. Liu, Y. Li, Y. Li, A. Pei, J. Xie, W. Huang, Y. Cui, *Nat. Chem.* **2019**, *11*, 382–389.
[7] K. Xu, *Chem. Rev.* **2004**, *104*, 4303–4417; J. Young, P. M. Kulick, T. R. Juran, M. Smeu, *ACS Appl. Energy Mater.* **2019**, *2*, 1676–1684.
[8] C. Yan, R. Xu, Y. Xiao, J. F. Ding, L. Xu, B. Q. Li, J. Q. Huang, *Adv. Funct. Mater.* **2020**, *30*, 1909887; R. Xu, X.-B. Cheng, C. Yan, X.-Q. Zhang, Y. Xiao, C.-Z. Zhao, J.-Q. Huang, Q. Zhang, *Matter* **2019**, *1*, 317–344; P. Verma, P. Maire, P. Novák, *Electrochim. Acta* **2010**, *55*, 6332–6341; H. Wang, Z. Yu, X. Kong, S. C. Kim, D. T. Boyle, J. Qin, Z. Bao, Y. Cui, *Joule* **2022**, *6*, 588–616; L. M. Suo, W. J. Xue, M. Gobet, S. G. Greenbaum, C. Wang, Y. M. Chen, W. L. Yang, Y. X. Li, J. Li, *Proc. Natl. Acad. Sci. USA* **2018**, *115*, 1156–1161; D.-J. Yoo, S. Yang, Y. S. Yun, J. H. Choi, D. Yoo, K. J. Kim, J. W. Choi, *Adv. Energy Mater.* **2018**, *8*, 1802365; Y. Sun, T. Yang, H. Ji, J. Zhou, Z. Wang, T. Qian, C. Yan, *Adv. Energy Mater.* **2020**, *10*, 2002373; L. Wang, A. Menakath, F. Han, Y. Wang, P. Y. Zavalij, K. J. Gaskell, O. Borodin, D. Iuga, S. P. Brown, C. Wang, K. Xu, B. W. Eichhorn, *Nat. Chem.* **2019**, *11*, 789–796; M. W. Swift, J. W. Swift, Y. Qi, *Nat. Comput. Sci.* **2021**, *1*, 212–220.
[9] K. Xu, *Chem. Rev.* **2014**, *114*, 11503–11618; X. D. Ren, P. Y. Gao, L. F. Zou, S. H. Jiao, X. Cao, X. H. Zhang, H. Jia, M. H. Engelhard, B. E. Matthews, H. P. Wu, H.-K. Lee, C. J. Niu, C. M. Wang, B. W. Arey, J. Xiao, J. Liu, J.-G. Zhang, W. Xu, *Proc. Natl. Acad. Sci. USA* **2020**, *117*, 28603–28613; A. von Wald Cresce, O. Borodin, K. Xu, *J. Phys. Chem. C* **2012**, *116*, 26111–26117; S. Li, W. Zhang, Q. Wu, L. Fan, X. Wang, X. Wang, Z. Shen, Y. He, Y. Lu, *Angew. Chem. Int. Ed.* **2020**, *59*, 14935–14941; *Angew. Chem.* **2020**, *132*, 15045–15051; T. Hou, G. Yang, N. N. Rajput, J. Self, S.-W. Park, J. Nanda, K. A. Persson, *Nano Energy* **2019**, *64*, 103881.
[10] X. Chen, X. Shen, B. Li, H.-J. Peng, X.-B. Cheng, B.-Q. Li, X.-Q. Zhang, J.-Q. Huang, Q. Zhang, *Angew. Chem. Int. Ed.* **2018**, *57*, 734–737; *Angew. Chem.* **2018**, *130*, 742–745; O. Borodin, X. M. Ren, J. Vatamanu, A. von Wald Cresce, J. Knap, K. Xu, *Acc. Chem. Res.* **2017**, *50*, 2886–2894; X. Chen, N. Yao, B.-S. Zeng, Q. Zhang, *Fundam. Res.* **2021**, *1*, 393–398; X. Chen, Q. Zhang, *Acc. Chem. Res.* **2020**, *53*, 1992–2002.
[11] X. Chen, H.-R. Li, X. Shen, Q. Zhang, *Angew. Chem. Int. Ed.* **2018**, *57*, 16643–16647; *Angew. Chem.* **2018**, *130*, 16885–16889.
[12] Z. Yu, H. Wang, X. Kong, W. Huang, Y. Tsao, D. G. Mackanic, K. Wang, X. Wang, W. Huang, S. Choudhury, Y. Zheng, C. V. Amanchukwu, S. T. Hung, Y. Ma, E. G. Lomeli,

J. Qin, Y. Cui, Z. Bao, *Nat. Energy* **2020**, *5*, 526–533; H. Zheng, H. Xiang, F. Jiang, Y. Liu, Y. Sun, X. Liang, Y. Feng, Y. Yu, *Adv. Energy Mater.* **2020**, *10*, 2001440; S. Liu, Q. Zhang, X. Wang, M. Xu, W. Li, B. L. Lucht, *ACS Appl. Mater. Interfaces* **2020**, *12*, 33719–33728; S. Nachimuthu, Z.-J. Tai, G. Brunklaus, J.-C. Jiang, *J. Phys. Chem. C* **2020**, *124*, 23523–23531; S. Zhang, G. Yang, Z. Liu, X. Li, X. Wang, R. Chen, F. Wu, Z. Wang, L. Chen, *Nano Lett.* **2021**, *21*, 3310–3317.

[13] Z. Yu, P. E. Rudnicki, Z. Zhang, Z. Huang, H. Celik, S. T. Oyakhire, Y. Chen, X. Kong, S. C. Kim, X. Xiao, H. Wang, Y. Zheng, G. A. Kamat, M. S. Kim, S. F. Bent, J. Qin, Y. Cui, Z. Bao, *Nat. Energy* **2022**, *7*, 94–106.

[14] Y. Jie, X. Ren, R. Cao, W. Cai, S. Jiao, *Adv. Funct. Mater.* **2020**, *30*, 1910777; X.-Q. Zhang, X. Chen, X.-B. Cheng, B.-Q. Li, X. Shen, C. Yan, J.-Q. Huang, Q. Zhang, *Angew. Chem. Int. Ed.* **2018**, *57*, 5301–5305; *Angew. Chem.* **2018**, *130*, 5399–5403; Y. Yamada, J. Wang, S. Ko, E. Watanabe, A. Yamada, *Nat. Energy* **2019**, *4*, 269–280; X. Cao, H. Jia, W. Xu, J. G. Zhang, *J. Electrochem. Soc.* **2021**, *168*, 010522.

[15] M. Baek, J. Kim, J. Jin, J. W. Choi, *Nat. Commun.* **2021**, *12*, 6807; S. Liu, X. Ji, N. Piao, J. Chen, N. Eidson, J. Xu, P. Wang, L. Chen, J. Zhang, T. Deng, S. Hou, T. Jin, H. Wan, J. Li, J. Tu, C. Wang, *Angew. Chem. Int. Ed.* **2021**, *60*, 3661–3671; *Angew. Chem.* **2021**, *133*, 3705–3715; Y. Liu, D. Lin, Y. Li, G. Chen, A. Pei, O. Nix, Y. Li, Y. Cui, *Nat. Commun.* **2018**, *9*, 3656.

[16] J.-F. Ding, R. Xu, N. Yao, X. Chen, Y. Xiao, Y.-X. Yao, C. Yan, J. Xie, J.-Q. Huang, *Angew. Chem. Int. Ed.* **2021**, *60*, 11442–11447; *Angew. Chem.* **2021**, *133*, 11543–11548; G. Yang, S. Zhang, S. Weng, X. Li, X. Wang, Z. Wang, L. Chen, *Nano Lett.* **2021**, *21*, 5316–5323; T. Li, X.-Q. Zhang, N. Yao, Y.-X. Yao, L.-P. Hou, X. Chen, M.-Y. Zhou, J.-Q. Huang, Q. Zhang, *Angew. Chem. Int. Ed.* **2021**, *60*, 22683–22687; *Angew. Chem.* **2021**, *133*, 22865–22869; Z. Wang, F. L. Qi, L. Yin, Y. Shi, C. Sun, B. An, H.-M. Cheng, F. Li, *Adv. Energy Mater.* **2020**, *10*, 1903843.

[17] C. F. N. Marchiori, R. P. Carvalho, M. Ebadi, D. Brandell, C. M. Araujo, *Chem. Mater.* **2020**, *32*, 7237–7246.

[18] X. Chen, X.-Q. Zhang, H.-R. Li, Q. Zhang, *Batteries Supercaps* **2019**, *2*, 128–131.

[19] N. Yao, X. Chen, X. Shen, R. Zhang, Z.-H. Fu, X.-X. Ma, X.-Q. Zhang, B.-Q. Li, Q. Zhang, *Angew. Chem. Int. Ed.* **2021**, *60*, 21473–21478; *Angew. Chem.* **2021**, *133*, 21643–21648.

[20] J. Chen, X. Fan, Q. Li, H. Yang, M. R. Khoshi, Y. Xu, S. Hwang, L. Chen, X. Ji, C. Yang, H. He, C. Wang, E. Garfunkel, D. Su, O. Borodin, C. Wang, *Nat. Energy* **2020**, *5*, 386–397; O. Sheng, J. Zheng, Z. Ju, C. Jin, Y. Wang, M. Chen, J. Nai, T. Liu, W. Zhang, Y. Liu, X. Tao, *Adv. Mater.* **2020**, *32*, 2000223; Y. Liu, X. Tao, Y. Wang, C. Jiang, C. Ma, O. Sheng, G. Lu, W. L. Xiong, *Science* **2022**, *375*, 739–745.

[21] J. Clarke-Hannaford, M. Breedon, T. Ruether, M. J. S. Spencer, *ACS Appl. Energy Mater.* **2020**, *3*, 5497–5509.

[22] C. L. Campion, W. Li, B. L. Lucht, *J. Electrochem. Soc.* **2005**, *152*, A2327–A2334; K. Tasaki, K. Kanda, S. Nakamura, M. Ue, *J. Electrochem. Soc.* **2003**, *150*, A1628–A1636.

[23] K. Sodeyama, Y. Yamada, K. Aikawa, A. Yamada, Y. Tateyama, *J. Phys. Chem. C* **2014**, *118*, 14091–14097; J. Qian, W. A. Henderson, W. Xu, P. Bhattacharya, M. Engelhard, O. Borodin, J. G. Zhang, *Nat. Commun.* **2015**, *6*, 6362; J. Wang, Y. Yamada, K. Sodeyama, C. H. Chiang, Y. Tateyama, A. Yamada, *Nat. Commun.* **2016**, *7*, 12032; S. R. Chen, J. M. Zheng, D. H. Mei, K. S. Han, M. H. Engelhard, W. G. Zhao, W. Xu, J. Liu, J.-G. Zhang, *Adv. Mater.* **2018**, *30*, 1706102; S. Perez Beltran, X. Cao, J.-G. Zhang, P. B. Balbuena, *Chem. Mater.* **2020**, *32*, 5973–5984; N. Piao, X. Ji, H. Xu, X. Fan, L. Chen, S. Liu, M. N. Garaga, S. G. Greenbaum, L. Wang, C. Wang, X. He, *Adv. Energy Mater.* **2020**, *10*, 1903568.

Manuscript received: July 23, 2022
Accepted manuscript online: October 31, 2022
Version of record online: November 24, 2022